atmosphere

MDPI

Article

Characteristics of Marine Heatwaves in the Indonesian Waters during the PDO, ENSO, and IOD Phases and Their Relationships to Net Surface Heat Flux

Erlin Beliyana [1], Nining Sari Ningsih [2,*], Sekar Ramdanira Gunawan [3] and Ayi Tarya [2]

[1] Doctoral Program in Earth Sciences, Faculty of Earth Sciences and Technology, Bandung Institute of Technology (ITB), Bandung 40132, Indonesia; erlinbeliyana99@gmail.com
[2] Research Group of Oceanography, Faculty of Earth Sciences and Technology, Bandung Institute of Technology (ITB), Bandung 40132, Indonesia; ayitarya@gmail.com
[3] Department of Oceanography, Faculty of Earth Sciences and Technology, Bandung Institute of Technology (ITB), Bandung 40132, Indonesia; sekargnwn@gmail.com
* Correspondence: nsningsih@itb.ac.id

Abstract: We conducted an investigation into the characteristics of marine heatwaves (MHWs) in Indonesian waters, aiming to understand the underlying mechanisms responsible for their formation, particularly the ones generated by net surface heat flux. To accomplish this, we utilized remote sensing data from the National Oceanic and Atmospheric Administration and the European Centre for Medium-Range Weather Forecasts. The dataset covered a 40-year period (1982–2021) encompassing both warm (1982–2007) and cold (2008–2021) phases of the Pacific Decadal Oscillation (PDO). Statistical analysis methods were employed to process the data. Our study reveals significant findings regarding MHWs in Indonesian waters. We observed the highest average frequency and maximum intensity of MHWs, occurring approximately 2–3 times a year and exceeding 1.5 °C, respectively, during the warm phase of PDO (with El Niño events occurring more frequently than La Niña). Conversely, the longest durations of MHWs in Indonesian waters were recorded during the cold phase of PDO (with La Niña events occurring more frequently than El Niño), spanning approximately 7–15 days. We identified local forcing in the form of net surface heat flux as the primary driver of MHW frequency and maximum intensity. During the warm phase of PDO, the net surface heat flux was notably higher, primarily due to increased shortwave radiation (heat gain) and reduced latent heat flux (heat loss) through the evaporation process. These factors collectively contributed to maintaining warmer ocean temperatures. Moreover, our study provides valuable insights into the interannual variability of MHWs through the application of composite calculations. We discovered a strong correlation between the occurrence of El Niño and positive Indian Ocean Dipole (IOD) events during the warm PDO phase and the highest frequency and maximum intensity of MHWs, with approximately 2.52 events and 1.54 °C, respectively. In contrast, we found that MHWs with the longest durations were closely linked to La Niña and negative IOD events during the cold PDO phase, lasting approximately 10.90 days. These findings highlight the complex interplay between climate phenomena and MHW characteristics, further deepening our understanding of their dynamics.

Keywords: global warming; marine heatwaves; Pacific Decadal Oscillation; ENSO; IOD; net surface heat flux; Indonesian waters

Citation: Beliyana, E.; Ningsih, N.S.; Gunawan, S.R.; Tarya, A. Characteristics of Marine Heatwaves in the Indonesian Waters during the PDO, ENSO, and IOD Phases and Their Relationships to Net Surface Heat Flux. *Atmosphere* **2023**, *14*, 1035. https://doi.org/10.3390/atmos14061035

Academic Editor: Vladimir Ivanov

Received: 19 April 2023
Revised: 29 May 2023
Accepted: 2 June 2023
Published: 16 June 2023

1. Introduction

Global warming continues to increase every year due to greenhouse gas emissions by human activities [1]. Over the past century, the global average air temperature has risen by 1.1 °C, highlighting the magnitude of this issue. The increasing air temperature has a profound impact on the oceans, as the intricate interaction between the atmosphere and the sea causes a rise in sea surface temperature (SST). This phenomenon is observed in

various regions worldwide, including Indonesia. According to [2], Indonesian waters have experienced a notable warming trend, with SST increasing by 0.19 ± 0.04 °C per decade over a 33-year period (1982–2014). This exceeds the average global SST warming trend of 0.13 °C per decade.

Areas with elevated SST are vulnerable to extreme events, such as tropical cyclones [3–5], intense rainfall, and even the occurrence of floods [6]. Another consequence of rising SST is the emergence of marine heatwaves (MHWs), characterized by prolonged periods of warm water anomalies (>90th percentile) lasting at least five consecutive days [7]. These MHWs have seen a global increase of over 50% [5] between 1925 and 2016 and are projected to persist until 2100 in most of the world's oceans, due to ongoing anthropogenic activities that contribute to further warming [8]. Furthermore, the frequency of MHWs has doubled since the 1980s, with a significant rise observed in 2021, especially in coastal areas [9]. MHWs can extend to depths surpassing 100 m [10–12] and exert a substantial influence on the dynamics of both the ocean and the atmosphere [6,13–16].

Additionally, MHWs have diverse effects on marine ecosystems, including instances of mass mortality, species migration, and shifts in ecosystem communities [17–22]. Moreover, MHWs have the capacity to alter various marine components, such as the carbon cycle and water column stratification, leading to reduced dissolved oxygen concentrations and inhibiting sea ice formation [23–26]. These alterations subsequently reinforce water column stratification in the ocean, which can weaken the mixing process and the upwelling strength. Consequently, this impact becomes evident in the diminished distribution of nutrients, phytoplankton, and zooplankton at the surface [27], ultimately resulting in a decline in fisheries resources and aquaculture production [4,28–30].

The occurrence of MHWs has been extensively documented worldwide in recent years, shedding light on their prevalence in various regions. Notable instances include MHWs observed in the Tasman Sea during 2015/16 [4], northern Australia in 2016 [31,32], the Gulf of Alaska and the Bering Sea in 2016 [32,33], California waters in 2016 [34], and the Tasman Sea in 2017/18 [35]. However, to the best of our knowledge, research on MHWs in Indonesian waters is relatively new, with limited investigations focused on local areas [36–39] and fishing management areas [40]. Furthermore, these studies primarily establish links between MHW characteristics and interannual SST signals of El Niño–Southern Oscillation (ENSO) and Indian Ocean Dipole (IOD), while neglecting the mechanisms contributing to MHW formation.

In recent years, extensive research has been conducted to comprehend the impact of ENSO and IOD on various oceanic phenomena apart from MHWs. Noteworthy studies on ENSO [41,42] have yielded valuable insights into its influence on Caspian seawater levels. While primarily focusing on the interaction between ENSO and sea level fluctuations, these investigations offer significant implications for understanding of the broader impacts of ENSO on oceanic processes. Particularly, these studies emphasize the role of El Niño events in elevating water levels in the Caspian Sea, attributed to changes in atmospheric circulation patterns and enhanced moisture transport to the region. Moreover, recent research has indicated the dominant role of ENSO and IOD in governing the interannual variation of the zonal current in the maritime continent (MC), specifically in the southern waters of Indonesia [43]. This study highlights that ENSO has the most substantial impact on the outflow of the Indonesian Throughflow (ITF), while the IOD's influence is particularly pronounced in southwestern Sumatra. Furthermore, the findings reveal a time lag, with ENSO leading the zonal current by approximately four months, while the IOD leads by approximately one month.

ENSO and IOD are the primary sources of interannual climate variability in the tropical Pacific and Indian Oceans, respectively. The relationship between these two phenomena is still a subject of debate, but there is evidence suggesting their interaction on a multidecadal time scale, such as Pacific Decadal Oscillation (PDO) and Atlantic Multidecadal Oscillation (AMO). The PDO is a longer-term SST pattern in the Pacific Ocean, typically spanning several decades (around 20 to 30 years) [44]. Its positive phase

corresponds to warmer SSTs in the northeastern Pacific and cooler SSTs in the central Pacific. On the other hand, the AMO is characterized by long-term fluctuations (ranging from 60 to 90 years) in SSTs in the North Atlantic Ocean, primarily influencing the Atlantic region [45]. Nevertheless, studies suggest that the AMO can indirectly influence SSTs in the Indo–Pacific region, including Indonesia, by altering atmospheric circulation patterns [45,46]. These multidecadal SST signals, such as PDO and AMO, play significant roles in shaping the climate patterns and variability in the Indo–Pacific region, including the MC, impacting rainfall patterns, temperature anomalies, atmospheric circulation, and ultimately affecting Indonesia's weather and climate [44–47].

The study conducted on marine heatwaves (MHWs) in Indonesian waters has not previously taken into account the influence of multidecadal SST signals. There is a lack of comprehensive knowledge regarding the specific characteristics of MHWs in Indonesian waters, including their differentiation based on the warm and cold phases of the PDO index pattern, as well as the underlying mechanisms driving MHW formation. Understanding these aspects is crucial in mitigating the impact of MHWs, especially considering the ongoing climate change affecting Indonesian waters. Therefore, the objective of this study is to further investigate the characteristics of MHWs, including their frequency, intensity, and duration, over the past 40 years (1982–2021) in Indonesian waters, distinguishing between the warm phase (1982–2007) and cold phase (2008–2021) of the PDO [48]. For the purposes of this study, we have focused solely on the PDO and have not included other decadal SST signals, such as the AMO, due to the lack of SST data specific to Indonesian waters required to capture its 60- to 90-year long-term fluctuations.

Moreover, comprehending the physical processes that underlie MHWs requires a crucial examination of the heat budget within the ocean mixed layer. Unfortunately, due to limited data availability regarding heat advection and diffusion in the Indonesian waters, the present study could not conduct a comprehensive heat budget calculation. Consequently, our investigation solely concentrates on the net surface heat flux, which is a contributing factor to the heat budget. Additionally, we explore the correlation between the net surface heat flux and the interdecadal variations in MHW characteristics based on the phases of the PDO. Furthermore, we analyze the components of the net surface heat flux that contribute the most to the development of MHWs. Although a more detailed analysis of the heat budget involving heat advection and diffusion falls beyond the scope of this study, it could be considered for future research. Accordingly, our study primarily focuses on the interannual and interdecadal variabilities of MHWs, particularly in relation to low-frequency fluctuations such as the ENSO, IOD, and PDO, as well as the contribution of the net surface heat flux to the MHW formation.

This paper is organized as follows. The "Materials and Methods" section provides a comprehensive description of the remote sensing and reanalysis data utilized in this study. In the "Results and Discussion" section, we present an overview of the interdecadal and interannual variability of MHWs from 1982–2021 and elaborate the mechanisms of MHW formation, which are primarily driven by local forcing in the form of net surface heat flux. Lastly, we end with a "Summary and Conclusions" section that highlights the main findings of our study.

2. Materials and Methods

To investigate the characteristics and factors contributing to the generation of MHWs within the Indonesian waters, this study utilized SST and atmospheric data. The study area encompassed the region between 8° N to 12° S and 95° E to 141° E, as shown in Figure 1. The data were collected from January 1982 to December 2021. The SST data used in this study were obtained from the National Oceanic and Atmospheric Administration (NOAA) Optimum Interpolation Sea Surface Temperature (OISST) dataset [49]. This dataset provides daily recordings with a spatial resolution of 0.25° × 0.25°. The net surface heat flux components, including shortwave radiation (SWR), longwave radiation (LWR), sensible heat flux (SHF), and latent heat flux (LHF), were derived from satellite imagery data

obtained from The European Center for Medium-Range Weather Forecasts (ECMWF) reanalysis data (ERA5), accessible at [50]. In this study, statistical analysis methods were applied to calculate the data for the entire 40-year period (1982–2021), as well as for the PDO warm phase (1982–2007) spanning 26 years and the PDO cold phase (2008–2021) covering 14 years. To determine the occurrences of ENSO, IOD, and neutral events, the Oceanic Niño Index (ONI) and Dipole Mode Index (DMI) were utilized for the period spanning 1982 to 2021 [51].

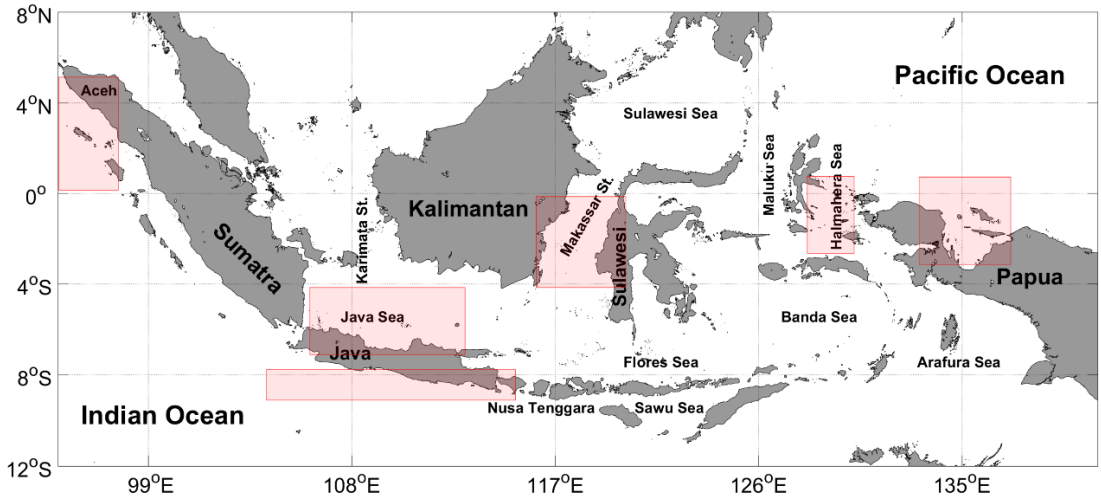

Figure 1. The area of study in the Indonesian waters (8° N to 12° S and 95° E to 141° E). The specific regions of interest are indicated by transparent red-colored squares: western region (western Sumatra and southern Java), inner seas (Java Sea and Makassar Strait), and eastern region (Halmahera Sea and northern Papua).

2.1. Identification of MHWs

In the present study, MHWs are defined as prolonged events of warm water anomalies that exceed a threshold (90th percentile) for at least five consecutive days [7]. To establish the climatology and threshold values, we calculated an 11-day window-centered average on each specific date spanning 40 years (1982–2021), 26 years (1982–2007), and 14 years (2008–2021). Following [7], a 30-day moving average was applied to generate a smooth climatology and threshold time series for MHWs. To analyze the interdecadal and interannual variabilities of MHWs and their relationship with PDO, ENSO, and IOD, we removed the long-term trend from the SST data. Spatial MHWs are detected and analyzed using a MATLAB toolbox provided by [52], accessible at [53]. Additionally, we focused on three metrics: frequency, maximum intensity, and duration. Frequency refers to the number of MHW occurrences, maximum intensity represents the highest temperature anomaly during MHWs, and duration defines the period when the temperature remains above the 90th percentile threshold without dipping below it for more than two consecutive days. Trends in the frequency, maximum intensity, and duration occurrences of MHWs were also calculated from January 1982 to December 2021.

2.2. Net Surface Heat Flux

To investigate the physical mechanism behind the formation of MHWs in the Indonesian waters, we analyzed the net surface heat flux, which is one of the contributing factors in the heat budget. The equation for the net surface heat flux can be expressed as follows:

$$Q_O = Q_{SWR} + Q_{LWR} + Q_{SHF} + Q_{LHF} \quad (1)$$

where Q_O is the net surface heat flux at the ocean surface, Q_{SWR} represents the shortwave radiation, also known as the surface net solar radiation, Q_{LWR} accounts for the longwave radiation, referred to as the surface net thermal radiation, Q_{SHF} represents the sensible

heat flux, which involves the transfer of heat between Earth's surface and the atmosphere through turbulent motion and is influenced by the temperature gradient between the sea and air, and Q_{LHF} denotes the latent heat flux, involving the transfer of heat between Earth's surface and the atmosphere through turbulent motion and is influenced by the humidity gradient between the sea and air [2,54]. To calculate the net surface heat flux, we initially removed the long-term trend from each component to isolate the interdecadal variability. Furthermore, we consider that positive fluxes indicate heat transfer from the atmosphere to the sea (heat gain), while negative fluxes indicate heat transfer from the ocean to the atmosphere (heat loss).

2.3. ONI and DMI Classification

In this study, we used the ONI and DMI to analyze the interannual variation of MHW characteristics and their relationship with the regional climate modes of ENSO and IOD. The ONI was utilized to monitor the phases of El Niño and La Niña, while the DMI was used to monitor positive and negative phases of IOD (pIOD and nIOD). The ONI is defined as the average SST anomalies in the Niño3.4 regions, spanning from 170° W to 120° W and 5° S to 5° N. On the other hand, the DMI is defined as the SST anomaly gradient between the western equatorial Indian Ocean (50° E–70° E, 10° S–10° N) and the southeastern equatorial Indian Ocean (90° E–110° E, 10° S–0°). El Niño and La Niña phases are determined when the ONI values exceeded 0.5 °C and fell below −0.5 °C, respectively [51]. Additionally, the pIOD phase was determined when DMI values exceeded 0.48 °C, while the nIOD phase was identified when the DMI values fell below −0.48 °C [55].

3. Results and Discussion

3.1. Characteristics of MHWs during the Cold and WARM Phases of PDO

In this study, we conducted an analysis of MHW characteristics based on three key metrics: frequency (Figure 2a–c), maximum intensity (Figure 2d–f), and duration of occurrence (Figure 2g–i) over different time periods. Specifically, we examined data spanning the last 40 years (1982–2021), with a focus on a 26-year warm phase of PDO (1982–2007) and a 14-year cold phase of PDO (2008–2021). The average frequency of MHW events over the 40-year period in Indonesian waters was found to be 2.10 events per year (Figure 2a). Notably, distinct patterns emerged when the PDO phases were considered separately. During the warm phase, the average MHW frequency was higher than in the cold phase (Figure 2b,c), with an average of 2.42 events per year (Figure 2b). Specifically, the Java and Halmahera Seas, Makassar Strait, and western Sumatra and northern Papua regions exhibited higher MHW frequencies compared to other areas (refer to Figure 1 for location details). Conversely, during the cold phase of PDO, the average frequency of MHWs significantly decreased to 1.51 events per year. In contrast to the warm phase, the Java and Halmahera Seas, Makassar Strait, and northern Papua displayed lower MHW frequencies during the cold phase, with only approximately one event per year (Figure 2c).

Figure 2d–f illustrates the characteristics of the MHWs in terms of their maximum intensity. The average maximum intensity of MHWs in Indonesian waters over a 40-year period is 1.49 °C (Figure 2d). During the warm (cold) phase of the PDO, as depicted in Figure 2e,f, the highest (lowest) average maximum intensity of MHWs was observed. Specifically, the warm and cold phases of PDO exhibited average MHW maximum intensities of 1.54 °C and 1.31 °C, respectively. The highest average maximum intensity areas during both phases were consistent across the three study periods mentioned earlier, mainly located in southern Java, exceeding 2 °C (Figure 2d–f). Furthermore, a previous study covering a shorter time span from January 1982 to December 2019 reported that the average maximum intensity in southern Java reached over 1.8 °C [36]. Interestingly, our present study reveals that the warm phase of the PDO, characterized by a higher frequency of El Niño events compared to La Niña events (Figure 2b,e), corresponds to the period with the highest occurrence of MHWs and their maximum intensity.

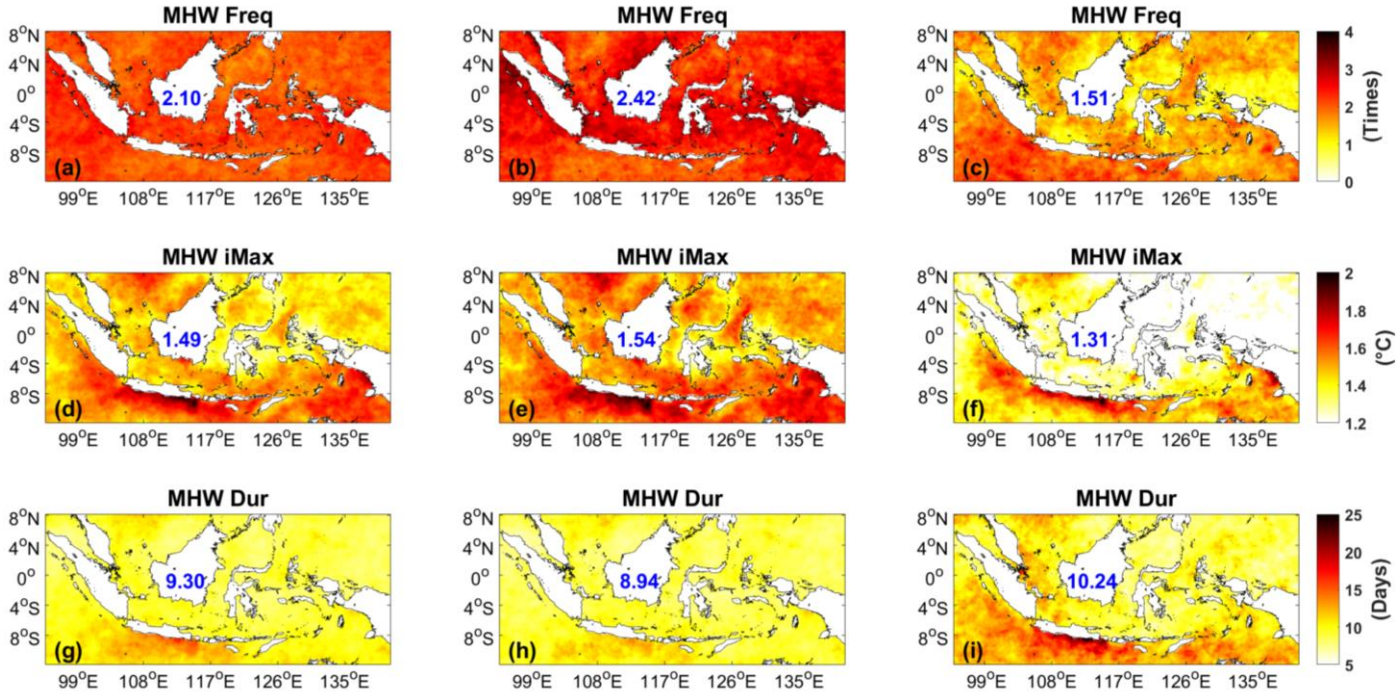

Figure 2. Statistical characteristics of the three metrics related to MHWs in the Indonesian waters over different time periods: 40 years (1982–2021; left panel), 26 years (1982–2007; PDO warm phase; middle panel), and 14 years (2008–2021; PDO cold phase; right panel). (**a**–**c**) Annual frequency of MHWs (in times), (**d**–**f**) Annual maximum intensity of MHWs (in °C), and (**g**–**i**) Annual duration of MHWs (in days).

Figure 2g–i display the duration of MHW occurrences. Over the last 40 years, Indonesian waters experienced an average MHW duration of 9.30 days (Figure 2g). Notably, the longest and shortest durations of MHWs were observed during the cold and warm phases, respectively, as shown in Figure 2i,h. In the cold phase, MHWs in Indonesian waters lasted between 10 and 20 days on average, with some instances exceeding 25 days in southern Java (Figure 2i). Conversely, during the warm phase of PDO, the average MHW duration was 8.94 days (Figure 2h). Regardless of the PDO phase or the 40-year timeframe, southern Java exhibited the longest durations and highest intensities of MHWs in Indonesian waters. These intense MHWs in southern Java have been classified as strong, severe, and even extreme, as explained by [36]. However, the underlying factors driving these strong MHWs in the southern Java region remain unresolved.

Our findings indicate that the cold phase of PDO, which corresponds to more La Niña years, is associated with the highest average duration of MHWs. During these conditions, positive SST anomalies are predominantly located in the western equatorial Pacific region. This localized warming may contribute to elevated temperatures in Indonesian waters through advection. However, the degree to which heat advection can influence MHWs in the Indonesian seas remains unresolved in the scope of this study. The complex topography and high tidal mixing in this region present challenges in accurately estimating heat advection using model outputs. These models may not faithfully replicate the SST patterns within the Indonesian seas, thereby complicating the estimation of heat advection. Furthermore, obtaining direct and long-term oceanic observations within the Indonesian seas is essential for improving our understanding of heat advection. However, acquiring such observations necessitates significant funding and support to bring this endeavor to fruition.

Furthermore, our findings suggest that the prolonged duration of MHWs observed during the past 14 years (2008–2021) within the PDO cold phase will likely lead to amplified ecological impacts in the following years. Conversely, the warm phase of PDO (which corresponds to more El Niño years) exhibits the highest average frequency and maximum

intensity of MHWs in the Indonesian waters. Several questions remain unanswered, including the factors influencing the frequency and maximum intensity of MHWs in these waters, as well as the underlying mechanism driving their development. In Section 3.4, we will further discuss these topics from an ocean–atmosphere interaction perspective, with particular emphasis on the net surface heat flux.

3.2. Composite Analysis of MHW Characteristics across Different Phases of PDO, ENSO, and IOD

In Section 3.1, we conducted an investigation into MHW characteristics in the Indonesian waters. To categorize the periods, we employed a rough approximation, where we considered the years 1982–2007 as the warm phase of the PDO and the years 2008–2021 as the cold phase of PDO. The grouping division of PDO phase was established with reference to [48]. However, the data presented in [48] reveals that the period identified as a warm phase of the PDO actually encompasses years classified as a cold PDO phase, and vice versa. Similarly, the same inconsistency applies to the phases of the ENSO, where a warm PDO phase may encompass both El Niño and La Niña events. Therefore, to gain a comprehensive understanding of the distinct impacts of various phases of the PDO, ENSO, and IOD on MHW characteristics in the study area, we conducted a repeated calculation of MHW metrics (including frequency, intensity, and duration) by using a composite analysis. This involved combining the respective variables across different phases of PDO, ENSO, and IOD, allowing us to obtain a clearer depiction of the constructive and destructive influences associated with each phase.

By assuming that the El Niño event is more frequent during PDO (+) or warm phase, while the El Niña event is more frequent during PDO (−) or cold phase, we have identified five notable occurrences that encompass different combinations of PDO, ENSO, and IOD phases, as shown in Table 1. It is worth noting that, in the dataset spanning from 1982 to 2021, we did not observe any instances of the combination involving PDO (+), El Niño, and nIOD.

Table 1. Various combinations of PDO, ENSO, and IOD phases for conducting a composite analysis of the three MHW metrics.

No.	Events
1.	PDO (+) and El Niño
2.	PDO (−) and La Niña
3.	PDO (+), El Niño, and pIOD
4.	PDO (−), La Niña, and pIOD
5.	PDO (−), La Niña, and nIOD

Figure 3 illustrates the MHW metrics in Indonesian waters for two specific combinations: PDO (+) and El Niño phases, as well as PDO (−) and La Niña phases. By specifically selecting El Niño years during the warm phase of the PDO, our analysis revealed significant findings. During this period, the annual frequency of MHWs was identified as 2.44 times, with the annual maximum intensity reaching 1.51 °C, and an average annual duration of 8.76 days (Figure 3a,c,e). Notably, even when focusing solely on the PDO (+) and El Niño phases, the occurrence of MHWs persists in Indonesian waters, suggesting that atmospheric heat sources may contribute to their formation in addition to oceanic influences.

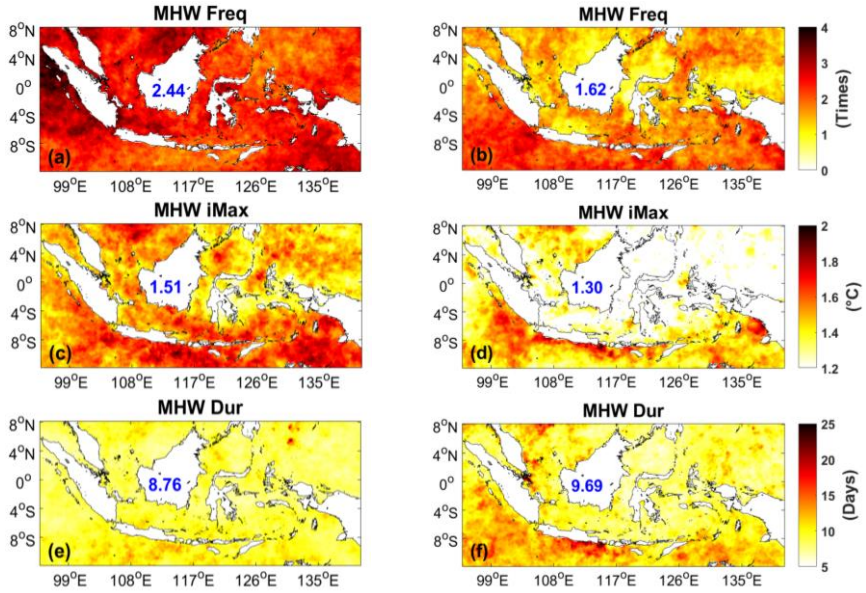

Figure 3. Composite analysis of the three MHW metrics in Indonesian waters over different time periods: PDO (+) and El Niño (left panel) and PDO (−) and La Niña (right panel). (**a**,**b**) Annual frequency (in times), (**c**,**d**) Annual maximum intensity (in °C), and (**e**,**f**) Annual duration (in days).

In contrast, when considering only La Niña years during the PDO (−) phase, the annual frequency of MHWs was found to be 1.62 times, with the annual maximum intensity reaching 1.30 °C, and an average annual duration of 9.69 days (Figure 3b,d,f). In this phase, the warm pool in the Pacific Ocean is typically located in the western equatorial region, near Indonesia. Therefore, ocean advection appears to support longer durations of MHWs in the study area. This composite analysis strengthens our previous approximation results (in Section 3.1), confirming that the frequency and maximum intensity of MHWs are higher during the PDO (+) and El Niño phases compared to the PDO (−) and La Niña phases. Conversely, the duration of MHWs during the PDO (−) and La Niña phases is longer than during the PDO (+) and El Niño phases.

We further refined the two specific combinations in Figure 3 by considering different IOD phases. The combination of El Niño years with pIOD events during the positive (warm) phase of the PDO produced significant results. In this particular scenario, all three metrics used to characterize MHWs exhibited higher values when compared to El Niño years alone, as shown in Figure 4a,d,g. Specifically, the annual frequency, annual maximum intensity, and annual duration were identified as 2.52 events, 1.54 °C, and 9.13 days, respectively. During this phase, the warm pool in the Pacific Ocean is typically observed in the Eastern Pacific Ocean adjacent to South America, while colder SSTs are observed in Indonesian waters relative to the western Indian Ocean during the pIOD. Despite the co-occurrence of El Niño and pIOD events during the positive PDO, which mutually reinforce each other and lead to the presence of cooler waters surrounding Indonesia, MHWs persisted in Indonesian waters with metric values that did not significantly differ from those observed during only El Niño events in the positive PDO. Unfortunately, we could not obtain the composite of MHW characteristics during the events of El Niño concurrent with nIOD during the positive PDO, as there were no such events recorded in our data period.

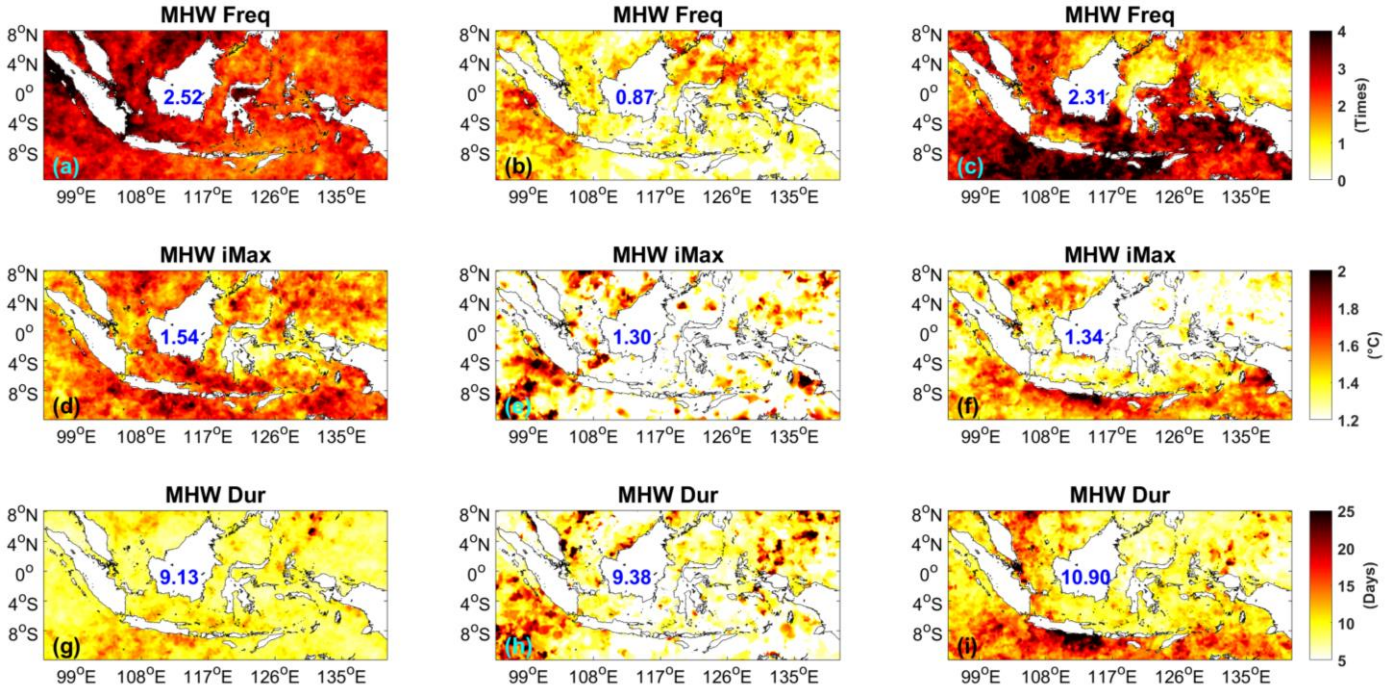

Figure 4. Same as in Figure 3 except for the combination of: PDO (+), El Niño, and pIOD (left panel), PDO (−), La Niña, and pIOD (middle panel), and PDO (−), La Niña, and nIOD (right panel).

Additionally, when La Niña years coincided with pIOD events during the negative (cold) phase of the PDO, the three MHW matrices reached their lowest values compared to the phases of La Niña alone or La Niña and nIOD during the negative PDO. The annual frequency, annual maximum intensity, and annual duration were recorded at 0.87 events, 1.30 °C, and 9.38 days, respectively (Figure 4b,e,h). Conversely, when La Niña events coincided with nIOD events during the cold phase of the PDO, noticeable increases were observed in all three MHW metrics compared to only La Niña years (Figure 3b,d,f). The annual frequency, annual maximum intensity, and annual duration reached values of 2.31 occurrences, 1.34 °C, and 10.90 days, respectively (Figure 4c,f,i). The simultaneous occurrence of La Niña and nIOD leads to warm conditions in Indonesian waters, with the influence of La Niña in the eastern part and the impact of nIOD in the western part. Consequently, the MHW metrics exhibit higher values during this phase, surpassing the magnitudes observed in La Niña years alone (Figure 3b,d,f).

The comparative analysis of composite calculations across the five distinct events reveals several key findings. Firstly, the spatial patterns of MHWs, including their frequency, maximum intensity, and duration, exhibit variations across different events. Additionally, the spatially averaged values of MHWs also differ among each event. The warm phase of the PDO, characterized by a higher occurrence of El Niño, significantly contributes to the increased frequency and maximum intensity of MHWs. In contrast, during the cold phase of the PDO, which is associated with a higher occurrence of La Niña, the frequency of MHWs is reduced, and their maximum intensity values are lower. However, the duration of MHWs is notably longer during this phase, particularly when the PDO is in the negative phase, combined with La Niña and nIOD. In fact, the average duration per year can reach up to 10.9 days, with the southern Java region exhibiting the longest durations, exceeding 25 days (refer to Figure 4i).

3.3. Linear Trend of MHWs during the Cold and Warm Phases of PDO

To quantify long-term trends of MHWs, we examined the linear trends in frequency (Figure 5a–c), maximum intensity (Figure 5d–f), and duration (Figure 5g–i). Black dots indicate areas, where increasing or decreasing events fell within the 90% confidence intervals

($p < 0.1$). On average, the MHW frequency has increased by approximately 1–1.65 events per decade over the past 40 years (Figure 5a), with occurrences observed across Indonesian waters. The majority of areas exhibited significant trends, as indicated by black dots covering all regions except for the Java and Flores Seas and southern Java. However, a few areas, such as western Sumatra and the coasts of southern Kalimantan and Sulawesi, demonstrated a decreasing trend in MHW frequency of around −0.95 event per decade. Notably, the frequency displayed varying increasing and decreasing trends during both warm and cold phases of the PDO (Figure 5b,c). Among the three study periods, the most substantial increase in frequency occurred during the cold phase, particularly in the northern territory of Indonesia waters, reaching up to 6.92 events per decade (Figure 5c). We anticipate this trend to persist, which is partly attributable to global warming. However, some areas, such as the Java Sea, western Sumatra, and southern Java, exhibited negative trends during the cold phase, with the most substantial decrease being −3.00 events per decade (see Figure 1 for location details). The maximum intensity of MHWs exhibited a negative linear trend over the past 40 years, with a decrease of −0.27 °C per decade (Figure 5d). During the PDO warm phase, there was a dominant decrease in the maximum intensity of MHWs, ranging from −0.10 to −0.58 °C per decade (Figure 5e). However, there were some localized areas with an increasing trend, albeit with low positive values of approximately 0.1 °C per decade in the Karimata and Makassar Straits, Sulawesi, Banda, and Arafura Seas. The southern Java region exhibited a higher increasing trend of 0.46 °C per decade (refer to Figure 1 for location details). Conversely, during the cold phase, the trend demonstrated greater variability, ranging from −0.75 to 0.75 °C per decade (Figure 5f). Positive trends were observed in the Karimata and Makassar Straits, the southern waters of Java to Nusa Tenggara, the Flores Sea, and the Maluku and Banda Seas, while other areas displayed negative trends (refer to Figure 1 for location details).

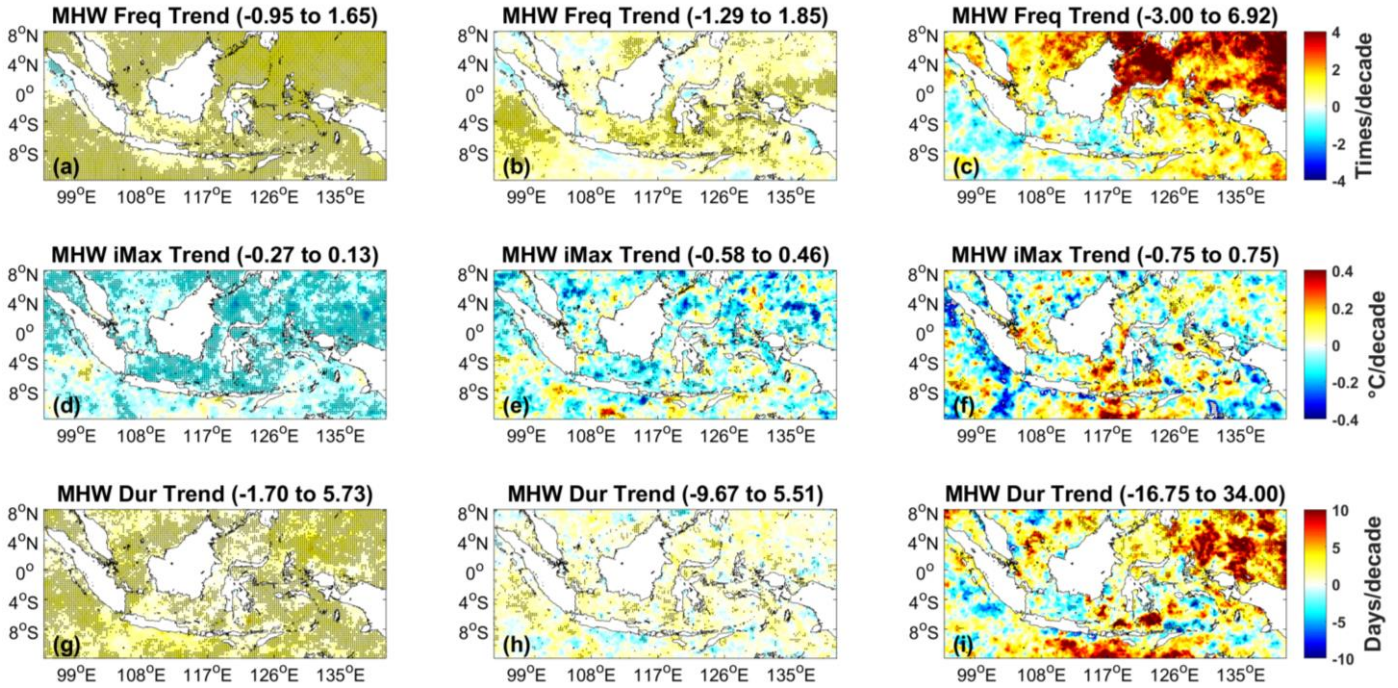

Figure 5. Spatial distribution of linear trend for the three MHW metrics in Indonesian waters over a period of 40 years (1982–2021; left panel), 26 years (1982–2007; PDO warm phase; middle panel), and 14 years (2008–2021; PDO cold phase; right panel). (**a**–**c**) MHW frequency (times/decade), (**d**–**f**) MHW maximum intensity (°C/decade), and (**g**–**i**) MHW duration (days/decade). Black dots represent locations with statistically significant trends ($p < 0.1$).

Figure 5g–i illustrate the linear trend of MHW duration. Over the last 40 years, the average duration of MHWs increased by three to four days per decade, with the highest trend recorded at 5.73 days per decade, as shown in Figure 5g. However, the pattern of the linear trend for MHW duration differed between the warm and cold phases of the PDO, as shown in Figure 5h,i. In the southern Java to Nusa Tenggara regions and the Flores Sea, as well as in the eastern Indonesian waters, particularly in the northern Maluku and Papua, the linear trend of MHW duration during the cold phase of PDO was notably higher than during the warm phase, predominantly exceeding 5 days per decade, with the highest value reaching 34 days per decade (Figure 5i). Conversely, during the warm phase of PDO, the linear trend of MHW duration was mainly below five days per decade (Figure 5h). Notably, when analyzing the PDO phases, all three MHW metrics exhibited a similar pattern in their linear trends, with the cold phase (characterized by more La Niña years) showing a stronger positive trend compared to the warm phase (characterized by more El Niño years). As discussed in Section 3.1, during La Niña years, positive SST anomalies are concentrated in the western equatorial Pacific region. This advection of warm water may contribute to the warming observed in Indonesian waters, thereby amplifying the trend in MHW characteristics.

3.4. The Formation of MHWs Generated by Local Forcing

3.4.1. Net Surface Heat Flux

Sea–atmosphere interactions in Indonesian waters are indicated by the net surface heat flux, which exhibits a positive value (Figure 6a–c). This positive value signifies a heat transfer process from the atmosphere to the sea, contributing to surface warming. Conversely, negative values of the net surface heat flux, observed south of the equator in the Indian Ocean at 12° S, indicate heat transfer from the sea to the atmosphere, resulting in sea cooling. Spatial variations in the net surface heat flux exhibit distinct patterns between the western and eastern regions of Indonesian waters during the three study periods (Figure 6a–c). Notably, this study reveals that the net surface heat flux is more pronounced in the eastern region compared to the western region. In the eastern region, the average net surface heat flux exceeds 80 W/m^2, with specific areas such as the Savu, Halmahera, and the Sulawesi Seas reaching values exceeding 100 W/m^2 (Figure 6a–c). On the other hand, the western region exhibits lower net surface heat flux ranging from 0–40 W/m^2, with negative values observed in the westernmost of the Aceh waters (~5 W/m^2) and the southern equatorial Indian Ocean (~20 W/m^2) throughout the three study periods (Figure 6a–c). The substantial difference in net surface heat flux characteristics between the eastern and western regions can be attributed to cloud cover. According to [56], the eastern region of Indonesian waters experiences lower total cloud cover compared to the western region due to seasonal influences. Moreover, the propagation of rain and cloud cover patterns typically occurs from west to east, leading to increased cloud cover in the western region. Consequently, this phenomenon impacts the amount of solar radiation reaching the sea, resulting in relatively limited solar radiation input in the western region compared to the eastern region of Indonesian waters.

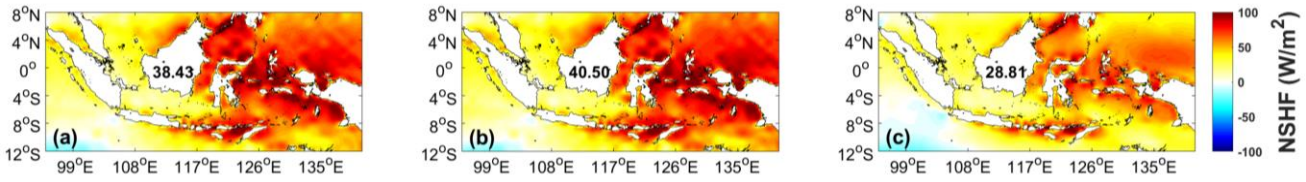

Figure 6. Net surface heat flux (NSHF) in Indonesian waters over (**a**) 40 years (1982–2021), (**b**) 26 years (1982–2007; PDO warm phase), and (**c**) 14 years (2008–2021; PDO cold phase).

In the three study periods, the highest net surface heat flux was observed during the warm phase of PDO, which coincides with more frequent El Niño events. The average net surface heat flux during this phase was 40.50 W/m^2 (Figure 6b). In contrast, during

the cold phase of PDO, characterized by more frequent La Niña events, and over the span of 40 years (1982–2021), the average net surface heat fluxes over Indonesian waters were 38.43 W/m^2 and 28.81 W/m^2, respectively.

During El Niño conditions, the western Pacific tends to be cooler than neutral, which can contribute to cooling in the Indonesian waters through advection. However, in the El Niño phase, atmospheric conditions over the Indonesian waters, particularly in the eastern regions, have the potential to reduce wind speed and cloud coverage. This, in turn, increases the net surface heat flux into the ocean, playing a role in ocean warming [57,58]. Therefore, the high frequency and maximum intensity of MHWs observed in the Indonesian waters during the warm phase of PDO (Figure 2b,e) were likely driven by air–sea heat flux rather than oceanic advection. This finding aligns with a previous study by [13], which highlighted the significant impact of the strong 2015/2016 El Niño on air–sea heat flux and the local atmosphere, resulting in the occurrence of large MHWs along the southeast coast of Queensland, Australia. These events led to structural ecosystem changes [59] and mass coral bleaching incidents [60].

3.4.2. Components of Net Surface Heat Flux

In this section, we will discuss the contribution of each surface heat flux component (SWR, LWR, SHF, and LHF) to the overall net surface heat flux, which has been proposed as a potential driver of the frequency and maximum intensity of MHWs. It is worth noting that SWR was the only component with a positive value, indicating heat transfer from the atmosphere into the ocean, while LWR, SHF, and LHF all had negative values, suggesting heat transfer from the ocean to the atmosphere and contributing to ocean cooling (refer to the scale values in Figure 7).

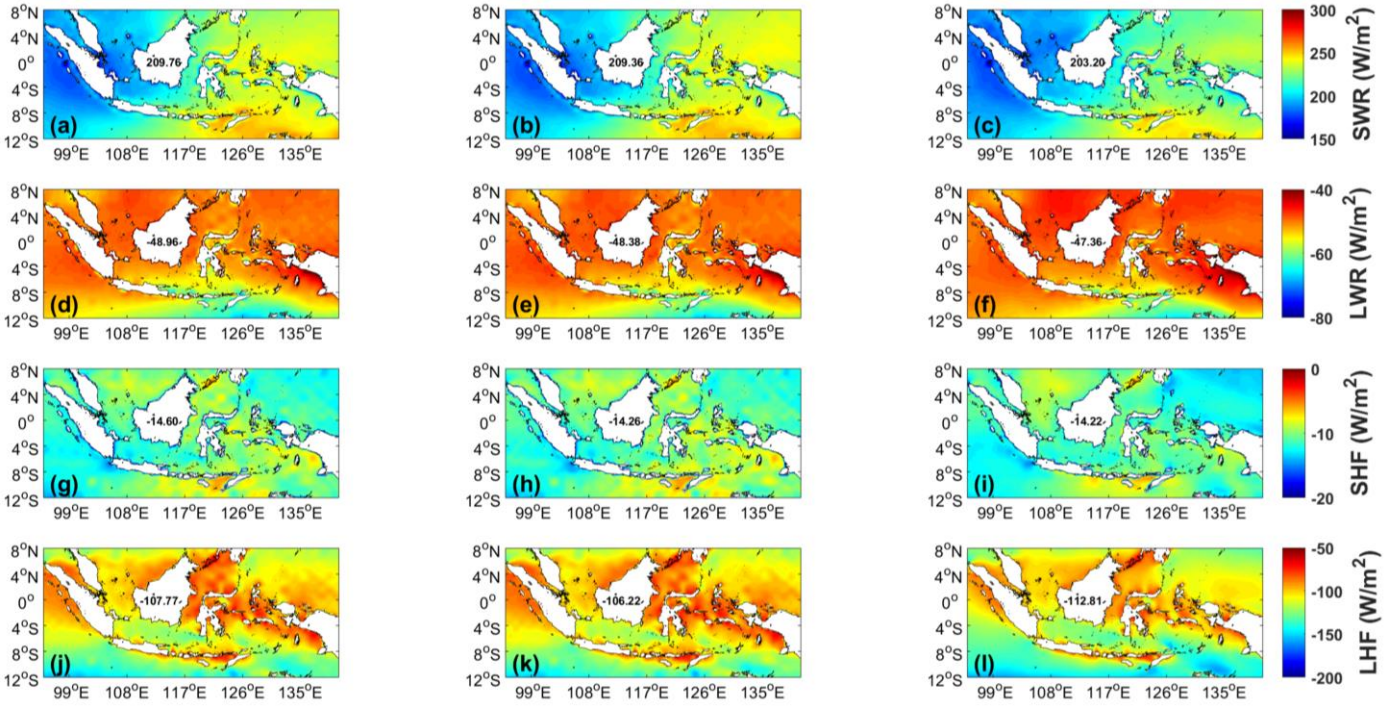

Figure 7. The values of SWR (**a**–**c**), LWR (**d**–**f**), SHF (**g**–**i**), and LHF (**j**–**l**) in units of W/m^2 for different time periods: a 40-year period (1982–2021; left panel), a 26-year period (1982–2007; middle panel; PDO warm phase), and a 14-year period (2008–2021; right panel; PDO cold phase).

Figure 7a–c depict the average SWR over the Indonesian waters for the 40-year period, as well as during the PDO warm and cold phases. The average SWR values were 209.76 W/m^2, 209.36 W/m^2, and 203.20 W/m^2, respectively, indicating a higher SWR during both the 40-year period and the PDO warm phase compared to the PDO cold phase.

Among the other components (LWR and SHF), LHF had the most significant contribution to heat loss, ranging from −50 to −150 W/m^2 (Figure 7j–l), while LWR and SHF contributed approximately −48 and −14 W/m^2, respectively (Figure 7d–i). Specifically, during the warm phase of PDO, the amount of LHF (heat loss) was smaller, at approximately −106.22 W/m^2 (Figure 7k), compared to the PDO cold phase, which reached −112.81 W/m^2 (Figure 7l). This suggests that low evaporation events influenced the reduced cloud cover, leading to higher SWR (heat gain) combined with lower LHF (heat loss) during the warm phase, resulting in a more substantial heat absorption by the ocean, as depicted in Figure 6b. Conversely, during the cold phase of PDO, increased evaporation (higher LHF) resulted in greater cloud formation, leading to a reduction in solar heat radiation reaching the ocean's surface (lower SWR) and consequently a lower value of net surface heat flux, as illustrated in Figure 6c.

3.5. Interannual Variations of MHWs

In this section, we conducted a detailed analysis of interannual variations in MHWs by considering the phases of ENSO and IOD within the timeframe of 1982 to 2021. The selection of each ENSO and IOD phase, including the neutral event, was based on the ONI and the DMI, as illustrated in Figure 8. Specifically, we identified seven significant events that encompassed various combinations of ENSO and IOD phases: El Niño and pIOD in 1997, El Niño and neutral IOD in 2016, neutral ENSO and pIOD in 2019, neutral ENSO and neutral IOD in 2013, neutral ENSO and nIOD in 1996, La Niña and neutral IOD in 1988, and La Niña and nIOD 1998. Among the selected periods, we focused on the most extreme event for each active phase of ENSO and IOD. For more detailed information on the classification of years where ENSO, IOD, and neutral events occurred between 1982 and 2021, please refer to Table 2.

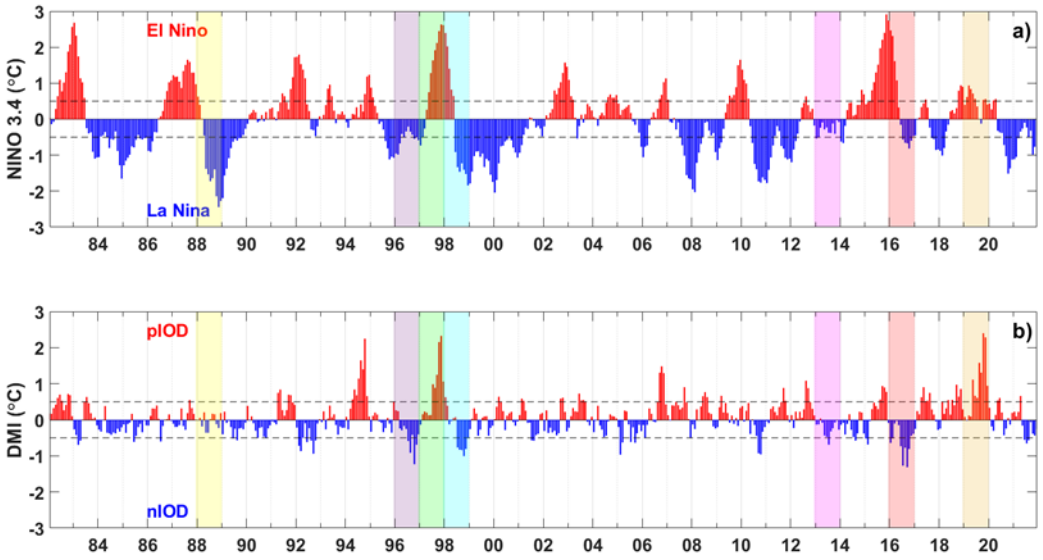

Figure 8. Temporal evolution of ONI and DMI during the period of 1982–2021. Dashed lines are depicted at the threshold values of (**a**) ±0.50 °C for ENSO qualification and (**b**) ±0.48 °C for IOD qualification. The red bars represent (**a**) El Niño and (**b**) pIOD events, whereas the blue bars indicate (**a**) La Niña and (**b**) nIOD events.

Table 2. The selected periods of ENSO, IOD, and neutral events within the timeframe of 1982 to 2021.

	pIOD	**Neutral**	**nIOD**
El Niño	1997	2016	-
Neutral	2019	2013	1996
La Niña	-	1988	1998

The results presented in the previous section clearly demonstrated that the warm phase of PDO, accompanied by more frequent El Niño events than La Niña, exhibited the highest frequency and maximum intensity of MHWs. However, it is important to note that each area within the Indonesian waters may exhibit distinct characteristics, as depicted in Figures 2 and 5.

Figure 2 provides valuable insights into the MHW frequency values, highlighting several areas of interest that exhibit an opposite pattern during the warm and cold phases of PDO. Specifically, these areas exhibit a notable increase in MHW frequency during the warm phase, while experiencing a corresponding decrease during the cold phase. These areas include six distinct regions, namely the western region (western Sumatra and southern Java), inner seas (Java Sea and Makassar Strait), and eastern region (Halmahera Sea and northern Papua), marked by the transparent red-colored squares in Figure 1. Consequently, to thoroughly investigate the interannual variations of MHW characteristics in relation to ENSO, IOD, and neutral events, an analysis was conducted on the frequency, maximum intensity, and total duration of MHWs. This analysis encompassed the six specified regions, as depicted in Figures 9–11. The primary objective of this investigation was to attain a comprehensive understanding of how MHWs vary across these regions in response to the aforementioned climatic drivers.

First, we examine the characteristics of MHWs during the neutral phases of ENSO and IOD. In 2013, during the neutral phase (denoted by the magenta bar in Figures 9–11), multiple MHWs were detected across all six areas. On average, the frequency, total duration, and maximum intensity of MHWs in these areas were 2.3 events, 19.3 days, and 0.89 °C, respectively.

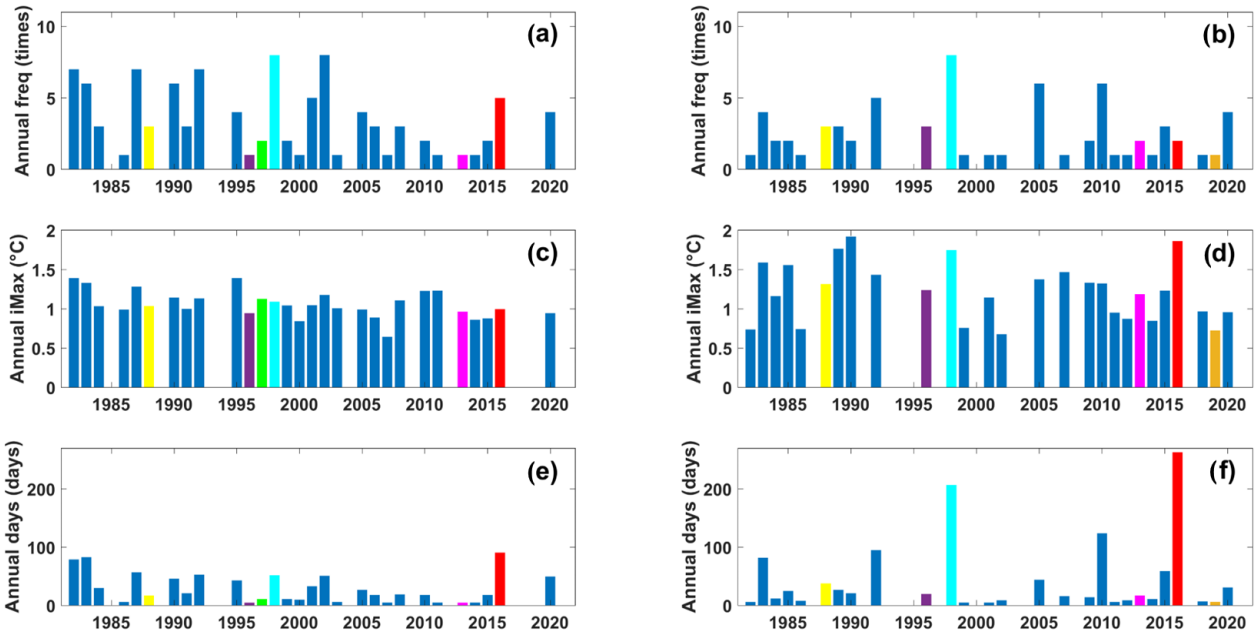

Figure 9. Annual averages of MHW characteristics in the western Sumatra (0.125° N–5.125° N, 94.875° E–97.875° E; left panel) and southern Java (7.875° S–9.125° S, 104.125° E–115.125° E; right panel) regions during the period of 1982–2021, with the long-term trend removed. (**a**,**b**) Annual frequency (in units of times), (**c**,**d**) Annual maximum intensity (in °C), and (**e**,**f**) Annual total duration (in days).

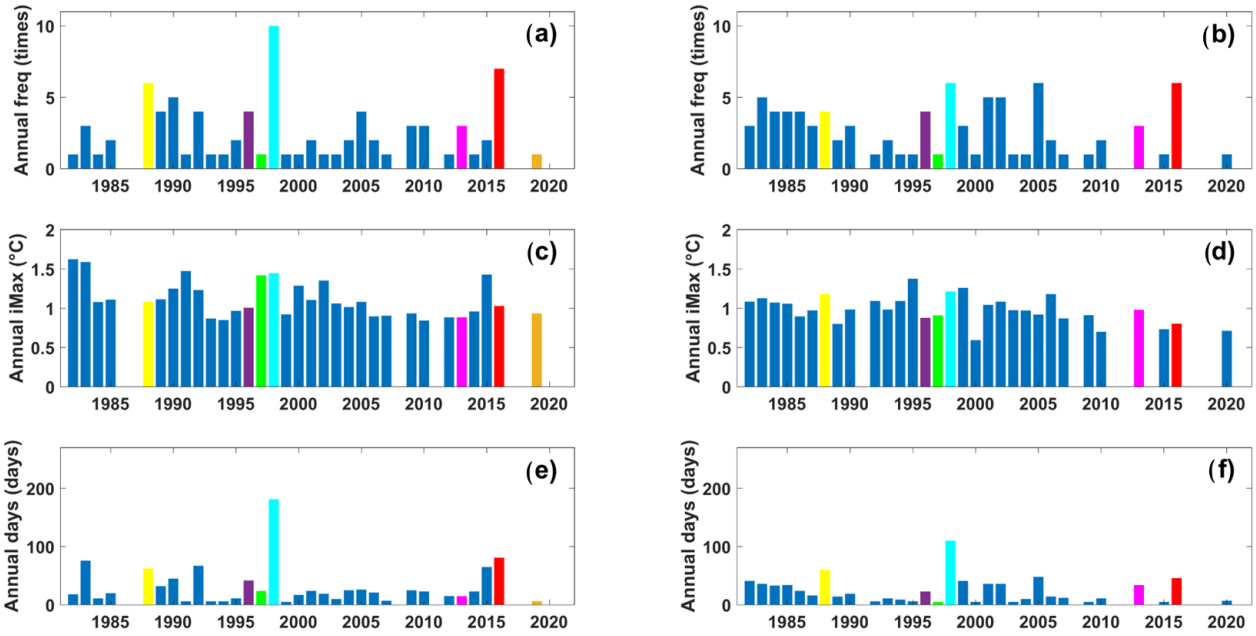

Figure 10. Same as in Figure 9 except for the Java Sea (4.125° S–7.125° S, 106.125° E–113.125° E; left panel) and the Makassar Strait (0.125° S–4.125° S, 116.125° E–120.125° E; right panel).

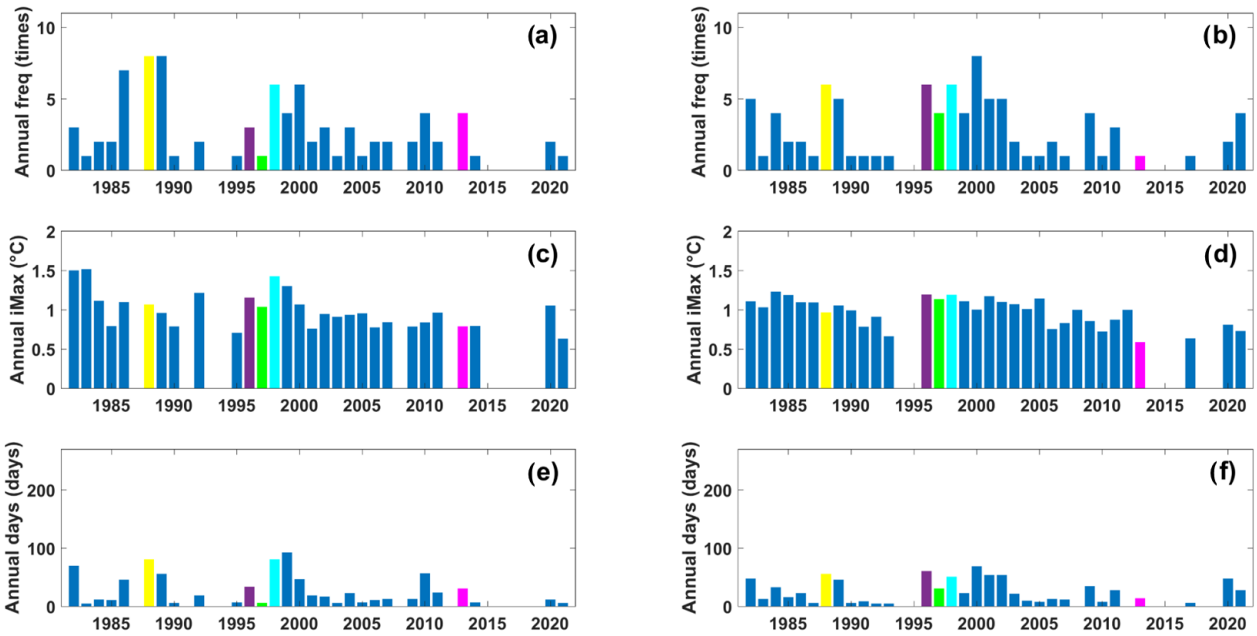

Figure 11. Same as in Figure 9 except for the Halmahera Sea (2.875° S–0.875° N, 128.125° E–130.125° E; left panel) and the northern Papua (3.125° S–0.875° N, 133.125° E–137.125° E; right panel).

Next, we compare the properties of MHWs during the positive and negative phases of ENSO and IOD with the neutral state. In 1988, during the La Niña and neutral IOD phases (denoted by the yellow bar in Figures 9–11), all six areas experienced several MHW events. On average, the frequency, total duration, and maximum intensity of MHWs during the La Niña phase were higher than during the neutral phase, reaching five events, 52.3 days, and 1.10 °C, respectively. Notably, in the Halmahera Sea, the highest frequency and longest duration of MHWs occurred during the La Niña phase, with eight events spanning 81 days (Figure 11a,c). Positive SST anomalies in the western equatorial Pacific during La Niña conditions [6] may contribute to warming in Indonesian waters through advection.

Previous studies have also highlighted the role of La Niña in the warming trend observed in the eastern Indonesian waters, such as the Makassar Strait and the Maluku and Banda Seas [2].

Meanwhile, during the El Niño and neutral IOD phases in 2016 (denoted by the red bar in Figures 9–11), several MHWs were detected in the western region and inner seas. However, no MHWs were observed in the eastern region (Figure 11). Interestingly, the western region (western Sumatra and southern Java) experienced the most prolonged MHW duration during the El Niño phase, lasting 91 and 263 days in western Sumatra and southern Java, respectively (Figure 9e,f). In southern Java, the highest maximum intensity of MHWs was also recorded in 2016, reaching 1.86 °C (Figure 9d). This represents the highest intensity of MHWs observed across all areas, nearly reaching 2 °C.

Furthermore, we analyzed the characteristics of MHWs during different phases of the IOD. During the nIOD and neutral ENSO phases in 1996 (denoted by the purple bar in Figures 9–11), all six areas regions experienced MHWs. The western region exhibited relatively short durations of 5 and 20 days (Figure 9e,f), with maximum intensity reaching 0.94 °C and 1.23 °C in western Sumatra and southern Java, respectively (Figure 9c,d). In contrast, the northern Papua region showed the longest total duration and the highest maximum intensity of MHWs during nIOD in 1996 compared to other IOD and ENSO phases (Figure 11d,f). According to [2], the nIOD led to SST warming in the western of Indonesian waters, particularly along the southern coast of Java and Sumatra, as well as in the Java and Flores Seas and Karimata Strait. Conversely, the fewest occurrences of MHWs were observed during the pIOD and neutral ENSO phases in 2019 (denoted by the brown bar in Figures 9–11), with only one MHW event identified in the Java Sea and southern Java, while other regions remained unaffected by MHWs. Both the Java Sea and southern Java experienced MHW duration of only six days (Figures 9f and 10e), reaching maximum intensities of 0.72 °C and 0.93 °C, respectively (Figures 9d and 10c).

Furthermore, we investigated the characteristics of MHWs during the simultaneous occurrence of ENSO and IOD phases, where their interactions can either attenuate or strengthen each other. First, we will examine the combination of La Niña and nIOD phases that took place in 1998 (denoted by the tosca bar in Figures 9–11). As depicted in Figures 9–11, a relatively high number of MHW events, averaging 7.3, occurred in all areas during this particular condition. Notably, within the inner seas (Java Sea and Makassar Strait), the highest three MHW metrics were observed in 1998 during the La Niña and nIOD phases (Figure 10). The total duration of MHWs surpassed 100 days in both areas, with 181 days in the Java Sea and 110 days in the Makassar Strait (Figure 10e,f), corresponding to 10 and 6 MHW events, respectively (Figure 10a,b). The maximum intensity of MHWs reached 1.44 °C in the Java Sea and 1.21 °C in the Makassar Strait (Figure 10c,d).

On the other hand, the combination of El Niño and pIOD phases in 1997 (indicated by the green bar in Figures 9–11) appeared to result in fewer occurrences of MHWs. Although MHWs were recorded in all areas except for the southern Java, the average frequency and total duration of MHWs were lower compared to the neutral phase, with only 1.8 events and 15.4 days, respectively.

Overall, both the La Niña and El Niño phases were found to significantly contribute to the development of MHWs compared to the neutral phase. This study highlights that during El Niño events, the net surface heat flux plays a crucial role in ocean warming. Conversely, during La Niña events, the advection of warm water from the western equatorial Pacific is suggested to enhance warming in Indonesian waters, leading to the generation of MHWs. Additionally, the presence of the nIOD condition was also found to favor MHW formation, while the pIOD condition had an adverse effect and could even induce cooling in Indonesian waters. As a result, a limited number of MHW events were observed during the pIOD phase, with only two out of the six areas (southern Java and Java Sea) experiencing MHWs during the 2019 pIOD event coinciding with the ENSO-neutral phase. Finally, the combination of La Niña and nIOD was identified as the most favorable condition for MHW formation, resulting in the highest frequency and maximum intensity of MHWs across

various areas in Indonesian waters, including western Sumatra, southern Java, the Java Sea, Makassar Strait, Halmahera Sea, and northern Papua, as previously described in this study.

The current study primarily focuses on investigating the interannual and interdecadal variabilities of MHWs, with a specific emphasis on their relationship with low-frequency modes such as ENSO, IOD, and PDO. While these low-frequency modes are essential, it is equally important to consider the factors that influence the seasonal and sub-seasonal variations of MHWs. Understanding these variations can offer valuable insights into extreme events, including heavy rainfall and tropical cyclones, that occur over the MC. Numerous studies have emphasized the impact of intraseasonal variability on surface temperature and precipitation changes across the MC. Notably, the Madden–Julian Oscillation (MJO), Boreal Summer Intraseasonal Oscillation (BSISO), and tropical waves have been identified as key factors that influence the region. These phenomena exhibit distinct patterns of atmospheric circulation, cloudiness, and precipitation, which can modulate the development and intensity of MHWs.

In a study by [61], the influence of convectively coupled equatorial waves (CCEWs) on precipitation variations across tropical regions, including the MC, was examined. The findings revealed that while CCEWs are less dominant compared to other tropical oscillations such as ENSO and MJO, they still contribute to 16–20% of the total intraseasonal precipitation variance, thereby impacting precipitation patterns. Furthermore, [62] investigated the influence of the MJO on precipitation in Indonesia and highlighted its significant role in modulating the frequency of extreme precipitation events in the country. Recent research by [63] emphasized the importance of considering the combined effects of both the MJO and convectively active phases of equatorial waves (Kelvin, TD-type, and eastward propagating inertia–gravity waves) on precipitation over the MC. Additionally, [64] provided further insights into the influence of the MJO and BSISO on precipitation in Indonesia. It is worth noting that these intraseasonal precipitation variations can affect surface air temperature, thereby potentially triggering the formation or suppression of MHWs. Consequently, these studies highlight the need to consider the interactions between tropical waves, atmospheric conditions, and oceanic processes when examining the variability of MHWs in Indonesian waters. While we acknowledge the significance of seasonal and sub-seasonal variations of MHWs and their implications for extreme events, our current study primarily concentrates on investigating the interannual and interdecadal variations of MHWs. However, we acknowledge the significance of exploring the seasonal and sub-seasonal variations of MHWs over the MC, and we intend to address this issue in future research.

4. Summary and Conclusions

This study assesses the characteristics of MHWs, including their frequency, maximum intensity, and duration of occurrences in the Indonesian waters over the last 40 years (1982–2021), specifically during a 26-year warm phase of PDO (1982–2007) and a 14-year cold phase of PDO (2008–2021). The analysis reveals that the longest average duration of MHWs, ranging from 7 to 15 days, occurred during the cold phase of PDO. On the other hand, the highest frequency (2–3 times per year) and maximum intensity (>1.5 °C) of MHWs were observed during the warm phase of PDO.

By examining five distinct events of PDO, ENSO, and IOD, the study highlights the spatial variability and varying values of frequency, maximum intensity, and duration of MHWs across these events. The warm phase of PDO, coupled with El Niño and pIOD events, exhibited the highest average frequency (2.52 events) and maximum intensity (1.54 °C) of MHWs. Conversely, the longest average duration of MHWs (10.90 days) was observed during the cold phase of PDO, coinciding with La Niña and nIOD events. Furthermore, the study reveals that the warm phase of PDO is associated with the highest net surface heat flux, which contributes to the elevated frequency and maximum intensity of MHWs during this phase. This condition is primarily driven by increased SWR as heat gain and reduced LHF as heat loss through the evaporation process.

At present, the ongoing cold phase of the PDO suggests that La Niña is expected to occur more frequently in the upcoming years, indicating a higher likelihood of increased MHW occurrences in Indonesia. The composite calculations yield similar results to the calculations of MHW characteristics when separated into the warm and cold phases of the PDO, albeit with some rough approximation. Specifically, during the warm phase of the PDO, the frequency and maximum intensity of MHWs are higher. Conversely, during the cold phase of the PDO, the duration of MHWs is typically longer.

Upon analyzing the interannual variability of MHWs influenced by ENSO and IOD, we found that both La Niña and El Niño phases significantly impact the development of MHWs in the Indonesian waters. Additionally, the nIOD phase also contributes to the MHW formation. Conversely, the occurrence of MHWs was less favorable during the pIOD phase, with only two out of the six regions, specifically southern Java and the Java Sea, experiencing MHWs.

Furthermore, this study investigated the characteristics of MHWs when ENSO and IOD phases reinforce or weaken each other. The findings revealed that the highest average frequency (7.3 days) and maximum intensity (1.35 °C) of MHWs in the six regions in Indonesian waters were observed in 1998, coinciding with the simultaneous occurrence of La Niña and the nIOD phase. Meanwhile, during the combination of El Niño and the pIOD phases in 1997, the frequency and duration of MHWs were lower compared to the neutral phase.

This study significantly enhances our understanding of various aspects related to MHWs in the Indonesian waters, including their characteristics, the role of net surface heat flux in their formation, as well as their interdecadal and interannual variabilities influenced by low-frequency climate modes, such as PDO, ENSO, and IOD. These findings contribute to the ongoing mitigation efforts aimed at addressing the MHW disaster in the Indonesian waters caused by climate change.

In order to fully understand the mechanisms behind MHWs, it is essential to thoroughly examine the heat budget within the ocean mixed layer. Regrettably, the lack of available data on heat advection and diffusion in the Indonesian waters prevented us from conducting a comprehensive calculation of the heat budget in the present study. Although this aspect is beyond the scope of our paper, it holds significant potential for future research endeavors. As a result, our investigation solely focuses on the net surface heat flux, which is a key component of the heat budget. In particular, we identified a notable disparity in the characteristics of net surface heat flux between the eastern and western Indonesian seas during the three study periods, which appears to play a contributing role in the formation of MHWs.

Additionally, while this study analyzed the comprehensive occurrence of MHWs on the surface of the Indonesian waters, it did not examine their presence in the subsurface. Further studies are necessary to investigate this phenomenon and gain a complete understanding of MHWs in the region, including their intraseasonal variabilities associated with the MJO and BSISO.

Author Contributions: E.B. methodology, writing—original draft, writing—review and editing, visualization; N.S.N. conceptualization, writing—review and editing, supervision, funding acquisition; S.R.G. methodology, writing—review and editing, visualization; and A.T. methodology, supervision. All authors have read and agreed to the published version of the manuscript.

Funding: Parts of this research were funded by Bandung Institute of Technology (ITB) under the program of Penelitian, Pengabdian kepada Masyarakat dan Inovasi ITB (P2MI) 2021 and 2022. This research was also supported by the Indonesian Ministry of Education, Culture, Research and Technology (Kemendikbudristek) under the research program of Penelitian Disertasi Doktor (PDD) 2022 (Research Grand Contract (RGC) No. 083/E5/PG.02.00.PT/2022) and 2023 (RGC No. 007/E5/PG.02.00/PL/2023).

Institutional Review Board Statement: Not applicable.

Informed Consent Statement: Not applicable.

Data Availability Statement: The SST data were obtained from https://www.ncei.noaa.gov/data/sea-surface-temperature-optimum-interpolation/v2.1/acess/avhrr/ (accessed on 21 December 2021). The surface heat flux components (shortwave radiation, longwave radiation, sensible heat flux, and latent heat flux) were available at https://cds.climate.copernicus.eu (accessed on 4 January 2022). Meanwhile, the ENSO and IOD indices were obtained from https://stateoftheocean.osmc.noaa.gov/ (accessed on 15 February 2022). A Matlab toolbox to detect and analyze the MHWs was sourced from https://github.com/ZijieZhaoMMHW/m_mhw1.0/ (accessed on 26 February 2022).

Acknowledgments: Parts of this research were funded by Bandung Institute of Technology (ITB) under the program of Penelitian, Pengabdian kepada Masyarakat dan Inovasi ITB (P2MI) 2021 and 2022. In addition, the authors are also very thankful to the Indonesian Ministry of Education, Culture, Research and Technology (Kemendikbudristek) for supporting this research under the research program of Penelitian Disertasi Doktor (PDD) 2022 and 2023. We also would like to gratefully acknowledge data support from NOAA and ECMWF.

Conflicts of Interest: The authors declare no conflict of interest.

References

1. IPCC. *Managing the Risks of Extreme Events and Disasters to Advance Climate Change Adaptation*; Cambridge University Press: Cambridge, UK, 2021; pp. 109–230. Available online: https://www.ipcc.ch/site/assets/uploads/2018/03/SREX-Chap3_FINAL-1.pdf (accessed on 5 March 2022).
2. Iskandar, I.; Mardiansyah, W.; Lestari, D.O.; Masumoto, Y. What did determine the warming trend in the Indonesian sea? *Prog. Earth Planet. Sci.* **2020**, *7*, 20. [CrossRef]
3. Kuleshov, Y.; Qi, L.; Fawcett, R.; Jones, D. On tropical cyclone activity in the Southern Hemisphere: Trends and the ENSO connection. *Geophys. Res. Lett.* **2008**, *35*, 1–5. [CrossRef]
4. Oliver, E.C.J.; Benthuysen, J.A.; Bindoff, N.L.; Hobday, A.J.; Holbrook, N.J.; Mundy, C.N.; Perkins-Kirkpatrick, S.E. The unprecedented 2015/16 Tasman Sea marine heatwave. *Nat. Commun.* **2017**, *8*, 16101. [CrossRef]
5. Oliver, E.C.J.; Donat, M.G.; Burrows, M.T.; Moore, P.J.; Smale, D.A.; Alexander, L.V.; Benthuysen, J.A.; Feng, M.; Gupta, A.S.; Hobday, A.J.; et al. Longer and more frequent marine heatwaves over the past century. *Nat. Commun.* **2018**, *9*, 1324. [CrossRef]
6. Behrens, E.; Fernandez, D.; Sutton, P. Meridional oceanic heat transport influences marine heatwaves in the Tasman Sea on interannual to decadal timescales. *Front. Mar. Sci.* **2019**, *6*, 228. [CrossRef]
7. Hobday, A.J.; Alexander, L.V.; Perkins-Kirkpatrick, S.E.; Smale, D.A.; Straub, S.C.; Oliver, E.C.J.; Benthuysen, J.A.; Burrows, M.T.; Donat, M.G.; Feng, M.; et al. A hierarchical approach to defining marine heatwaves. *Prog. Oceanogr.* **2016**, *141*, 227–238. [CrossRef]
8. Frölicher, T.L.; Fischer, E.M.; Gruber, N. Marine heatwaves under global warming. *Nature* **2018**, *560*, 360–364. [CrossRef]
9. IPCC. *Intergovernmental Panel on Climate Change, Climate Change 2021: Impacts, Adaptation, and Vulnerability*; Cambridge University Press: Cambridge, UK, 2021. Available online: https://report.ipcc.ch/ar6/wg2/IPCC_AR6_WGII_FullReport.pdf (accessed on 11 March 2022).
10. Pearce, A.F.; Feng, M. The rise and fall of the "marine heat wave" off Western Australia during the summer of 2010/2011. *J. Mar. Syst.* **2013**, *111–112*, 139–156. [CrossRef]
11. Jackson, J.M.; Johnson, G.C.; Dosser, H.V.; Ross, T. Warming from recent marine heatwave lingers in deep British Columbia fjord. *Geophys. Res. Lett.* **2018**, *45*, 9757–9764. [CrossRef]
12. Su, Z.; Pilo, G.S.; Corney, S.; Holbrook, N.J.; Mori, M.; Ziegler, P. Characterizing marine heatwaves in the Kerguelen Plateau region. *Front. Mar. Sci.* **2021**, *7*, 531297. [CrossRef]
13. Heidemann, H.; Ribbe, J. Marine heat waves and the influence of El Niño off Southeast Queensland, Australia. *Front. Mar. Sci.* **2019**, *6*, 56. [CrossRef]
14. Feng, X.; Shinoda, T. Air-sea heat flux variability in the Southeast Indian Ocean and its relation with Ningaloo Niño. *Front. Mar. Sci.* **2019**, *6*, 266. [CrossRef]
15. Fewings, M.R.; Brown, K.S. Regional structure in the marine heat wave of summer 2015 off the Western United States. *Front. Mar. Sci.* **2019**, *6*, 564. [CrossRef]
16. Gawarkiewicz, G.; Chen, K.; Forsyth, J.; Bahr, F.; Mercer, A.M.; Ellertson, A.; Fratantoni, P.; Seim, H.; Haines, S.; Han, L. Characteristics of an advective marine heatwave in the Middle Atlantic Bight in early 2017. *Front. Mar. Sci.* **2019**, *6*, 712. [CrossRef]
17. Fordyce, A.J.; Ainsworth, T.D.; Heron, S.F.; Leggat, W. Marine heatwave hotspots in coral reef environments: Physical drivers, ecophysiological outcomes and impact upon structural complexity. *Front. Mar. Sci.* **2019**, *6*, 498. [CrossRef]
18. Kendrick, G.A.; Nowicki, R.J.; Olsen, Y.S.; Strydom, S.; Fraser, M.W.; Sinclair, E.A.; Statton, J.; Hovey, R.K.; Thomson, J.A.; Burkholder, D.A.; et al. A Systematic review of how multiple stressors from an extreme event drove ecosystem-wide loss of resilience in an iconic seagrass community. *Front. Mar. Sci.* **2019**, *6*, 455. [CrossRef]
19. Smale, D.A.; Wernberg, T.; Oliver, E.C.J.; Thomsen, M.; Harvey, B.P.; Straub, S.C.; Burrows, M.T.; Alexander, L.V.; Benthuysen, J.A.; Donat, M.G.; et al. Marine heatwaves threaten global biodiversity and the provision of ecosystem services. *Nat. Clim. Chang.* **2019**, *9*, 306–312. [CrossRef]

20. Smith, K.A.; Dowling, C.E.; Brown, J. Simmered then boiled: Multi decadal poleward shift in distribution by a temperate fish accelerates during marine heatwave. *Front. Mar. Sci.* **2019**, *6*, 407. [CrossRef]
21. Strub, P.T.; James, C.; Montecino, V.; Rutllant, J.A.; Blanco, J.L. Ocean circulation along the Southern Chile transition region (38°–46°S): Mean, seasonal and interannual variability, with a focus on 2014–2016. *Prog. Oceanog.* **2019**, *172*, 159–198. [CrossRef]
22. Thomsen, M.S.; Mondardini, L.; Alestra, T.; Gerrity, S.; Tait, L.; South, P.; Lilley, S.A.; Sciel, D.R. Local extinction of bull kelp (*Durvillaea* spp.) due to a marine heatwave. *Front. Mar. Sci.* **2019**, *6*, 84. [CrossRef]
23. Brauko, K.M.; Cabral, A.; Costa, N.V.; Hayden, J.; Dias, C.E.P.; Leite, E.S.; Westphal, R.D.; Mueller, C.M.; Hall-Spencer, J.M.; Rodrigues, R.R.; et al. Marine heatwaves, sewage and eutrophication combine to trigger deoxygenation and biodiversity loss: A SW Atlantic case study. *Front. Mar. Sci.* **2020**, *7*, 590258. [CrossRef]
24. Hu, S.; Zhang, L.; Qian, S. Marine heatwaves in the Arctic region: Variation in different ice covers. *Geophys. Res. Lett.* **2020**, *47*, e2020GL089329. [CrossRef]
25. Carvalho, K.S.; Smith, T.E.; Wang, S. Bering Sea marine heatwaves: Patterns, trends and connections with the Arctic. *J. Hydrol.* **2021**, *600*, 126462. [CrossRef]
26. Mignot, A.; Schuckmann, K.V.; Gasparin, F.; Gennip, S.V.; Landschützer, P.; Perruche, C.; Lamouroux, J.; Amm, T. Decrease in air-sea CO2 fluxes caused by persistent marine heatwaves. *Nat. Commun.* **2021**, *13*, 4300. [CrossRef] [PubMed]
27. Doney, S.C. Plankton in warmer world. *Nature* **2006**, *444*, 695–696. [CrossRef]
28. Mills, K.; Pershing, A.; Brown, C.; Chen, Y.; Chiang, F.S.; Holland, D. Fisheries management in a changing climate: Lessons from the 2012 ocean heat wave in the Northwest Atlantic. *Oceanography* **2013**, *26*, 191–195. [CrossRef]
29. Caputi, N.; Kangas, M.; Denham, A.; Feng, M.; Pearce, A.; Hetzel, Y.; Chandrapavan, A. Management adaptation of invertebrate fisheries to an extreme marine heat wave event at a global warming hot spot. *Ecol. Evol.* **2016**, *6*, 3583–3593. [CrossRef]
30. Cheung, W.W.L.; Frölicher, T.L. Marine heatwaves exacerbate climate change impacts for fisheries in the Northeast Pacific. *Sci. Rep.* **2020**, *10*, 6678. [CrossRef]
31. Lewis, S.C.; Mallela, J. A multifactor risk analysis of the record 2016 great barrier reef bleaching. *Bull. Am. Meteorol. Soc.* **2018**, *99*, S144–S149. [CrossRef]
32. Oliver, E.C.J.; Perkins-Kirkpatrick, S.E.; Holbrook, N.J.; Bindoff, N.L. Anthropogenic influences on record 2016 marine heatwave. *Bull. Am. Meteorol. Soc.* **2018**, *99*, S44–S48. [CrossRef]
33. Walsh, J.E.; Thoman, R.L.; Bhatt, U.S.; Bieniek, P.A.; Brettschneider, B.; Brubaker, M.; Danielson, S.; Lader, R.; Fetterer, F.; Holderied, K.; et al. The high latitude marine heat wave of 2016 and its impacts on Alaska. *Bull. Am. Meteorol. Soc.* **2018**, *99*, S39–S43. [CrossRef]
34. Jacox, M.G.; Alexander, M.A.; Mantua, N.J.; Scott, J.D.; Hervieux, G.; Webb, R.S.; Werner, F.E. Forcing of multiyear extreme ocean temperatures that impact California current living marine resources in 2016. *Bull. Am. Meteorol. Soc.* **2018**, *99*, S27–S33. [CrossRef]
35. Perkins-Kirkpatrick, S.; King, A.; Cougnon, E.; Grose, M.; Oliver, E.C.J.; Holbrook, N.J.; Lewis, S.C.; Pourasghar, F. The role of natural variability and anthropogenic climate change in the 2017/18 Tasman Sea marine heatwave. *Bull. Am. Meteorol. Soc.* **2019**, *100*, S105–S110. [CrossRef]
36. Iskandar, M.; Ismail, M.F.A.; Arifin, T.; Chandra, H. Marine heatwaves of sea surface temperature off South Java. *Heliyon* **2021**, *7*, e08618. [CrossRef]
37. Ismail, M.F.A. Characteristics of marine heatwaves off West Sumatra derived from high-resolution satellite data. *J. Hunan Univ. Nat. Sci.* **2021**, *48*, 130–136.
38. Beliyana, E.; Ningsih, N.S.; Tarya, A. Characteristics of marine heatwaves (2008–2021) in the Savu Sea, East Nusa Tenggara. *J. Phys. Conf. Ser.* **2022**, *2377*, 012043. [CrossRef]
39. Gunawan, S.R.; Ningsih, N.S.; Beliyana, E.; Tarya, A. Marine heatwaves characteristics in Spermonde Islands, west coast of South Sulawesi, Indonesia. *J. Phys. Conf. Ser.* **2022**, *2377*, 012040. [CrossRef]
40. Habibullah, A.D.; Tarya, A.; Ningsih, N.S.; Putri, M.R. Marine heatwaves in the Indonesian fisheries management areas. *J. Mar. Sci. Eng.* **2023**, *11*, 161. [CrossRef]
41. Molavi-Arabshahi, M.; Arpe, K. Interactions between the Caspian Sea size (level) and atmospheric circulation. *Int. J. Climatol.* **2022**, *42*, 9626–9640. [CrossRef]
42. Arpe, K.; Molavi-Arabshahi, M.; Leroy, S.A.G. Wind variability over the Caspian Sea, its impact on Caspian seawater level and link with ENSO. *Int. J. Climatol.* **2020**, *40*, 6039–6054. [CrossRef]
43. Ningsih, N.S.; Sakina, S.L.; Susanto, R.D.; Hanifah, F. Simulated zonal current characteristics in the southeastern tropical Indian Ocean (SETIO). *Ocean Sci.* **2021**, *17*, 1115–1140. [CrossRef]
44. Yao, J.; Xiao, L.; Gou, M.; Li, C.; Lian, E.; Yang, S. Pacific decadal oscillation impact on East China precipitation and its imprint in new geological documents. *Sci. China Earth Sci.* **2018**, *61*, 473–482. [CrossRef]
45. Knudsen, M.F.; Seidenkrantz, M.S.; Jacobsen, B.H.; Kuijpers, A. Tracking the Atlantic Multidecadal Oscillation through the last 8000 years. *Nat. Commun.* **2011**, *2*, 178. [CrossRef] [PubMed]
46. Kucharski, F.; Parvin, A.; Rodriguez-Fonseca, B.; Farneti, R.; Martin-Rey, M.; Polo, I.; Mohino, E.; Losada, T.; Mechoso, C.R. The Teleconnection of the tropical Atlantic to Indo-Pacific sea surface temperatures on inter-annual to centennial time scales: A review of recent findings. *Atmosphere* **2016**, *7*, 29. [CrossRef]

47. Shi, L.; Zhang, J.; Zhang, D.; Wang, J.; Meng, X.; Liu, Y.; Yao, F. What caused the interdecadal shift in the El Niño–Southern Oscillation (ENSO) impact on dust mass concentration over northwestern South Asia? *Atmos. Chem. Phys.* **2022**, *22*, 11255–11274. [CrossRef]
48. PDO Index. Available online: https://www.daculaweather.com/4_pdo_index.php (accessed on 15 February 2022).
49. SST Dataset. Available online: https://www.ncei.noaa.gov/data/sea-surface-temperature-optimum-interpolation/v2.1/acess/avhrr/ (accessed on 21 December 2021).
50. ECMWF Dataset. Available online: https://cds.climate.copernicus.eu (accessed on 4 January 2022).
51. ENSO and IOD Indices. Available online: https://stateoftheocean.osmc.noaa.gov/ (accessed on 15 February 2022).
52. Zhao, Z.; Marin, M.A. MATLAB toolbox to detect and analyze marine heatwaves. *J. Open Source Softw.* **2019**, *4*, 1124. [CrossRef]
53. MATLAB Toolbox. Available online: https://github.com/ZijieZhaoMMHW/m_mhw1.0/ (accessed on 26 February 2022).
54. Pujol, C.; Pérez-Santos, I.; Barth, A.; Alvera-Azcárate, A. Marine heatwaves offshore Central and South Chile: Understanding forcing mechanisms during the years 2016–2017. *Front. Mar. Sci.* **2022**, *9*, 800325. [CrossRef]
55. Pant, V.; Girishkumar, M.S.; Bhaskar, T.V.S.U.; Ravichandran, M.; Papa, F.; Thangaprakash, V.P. Observed interannual variability of near-surface salinity in the Bay of Bengal. *J. Geophys. Res. Oceans* **2015**, *120*, 3315–3329. [CrossRef]
56. Wallace, J.M.; Hobbs, P.V. *Atmospheric Science: An Introduction Survey*, 2nd ed.; Elsevier: Amsterdam, The Netherland, 2006; pp. 352–353, 357, 367–368.
57. Feng, M.; McPhaden, M.J.; Xie, S.P.; Hafner, J. La Niña forces unprecedented Leeuwin Current warming in 2011. *Sci. Rep.* **2013**, *3*, 1277. [CrossRef]
58. Zhang, L.; Han, W.; Li, Y.; Shinoda, T. Mechanisms for generation and development of Ningaloo Niño. *J. Clim.* **2018**, *31*, 9239–9259. [CrossRef]
59. Stuart-Smith, R.D.; Brown, C.J.; Ceccarelli, D.M.; Edgar, G.J. Ecosystem restructuring along the Great Barrier Reef following mass coral bleaching. *Nature* **2018**, *560*, 92–96. [CrossRef]
60. Benthuysen, J.A.; Oliver, E.C.J.; Feng, M.; Marshall, A.G. Extreme Marine Warming Across tropical Australia during austral summer 2015–2016. *J. Geophys. Res. Oceans* **2018**, *123*, 1301–1326. [CrossRef]
61. Lubis, S.W.; Jacobi, C. The modulating influence of convectively coupled equatorial waves (CCEWs) on the variability of tropical precipitation. *Int. J. Climatol.* **2015**, *35*, 1465–1483. [CrossRef]
62. Muhammad, F.R.; Lubis, S.W.; Setiawan, S. Impacts of the Madden–Julian oscillation on precipitation extremes in Indonesia. *Int. J. Climatol.* **2020**, *41*, 1970–1984. [CrossRef]
63. Lubis, S.W.; Hagos, S.; Hermawan, E.; Respati, M.R.; Ridho, A.; Risyanto; Paski, J.A.I.; Muhammad, F.R.; Siswanto; Ratri, D.N.; et al. Record-breaking precipitation in Indonesia's Capital of Jakarta in early January 2020 linked to the northerly surge, equatorial waves, and MJO. *Geophys. Res. Lett.* **2022**, *49*, e2022GL101513. [CrossRef]
64. Muhammad, F.R.; Lubis, S.W. Impacts of the boreal summer intraseasonal oscillation on precipitation extremes in Indonesia. *Int. J. Climatol.* **2023**, *43*, 1576–1592. [CrossRef]